

Molecular dynamics simulation of radiation damage in CaCd6 quasicrystal cubic approximant up to 10 keV

P. H. Chen, K. Avchachov, K. Nordlund, and K. Pussi

Citation: *J. Chem. Phys.* **138**, 234505 (2013); doi: 10.1063/1.4811183

View online: <http://dx.doi.org/10.1063/1.4811183>

View Table of Contents: <http://jcp.aip.org/resource/1/JCPSA6/v138/i23>

Published by the AIP Publishing LLC.

Additional information on J. Chem. Phys.

Journal Homepage: <http://jcp.aip.org/>

Journal Information: http://jcp.aip.org/about/about_the_journal

Top downloads: http://jcp.aip.org/features/most_downloaded

Information for Authors: <http://jcp.aip.org/authors>

ADVERTISEMENT



physicstoday

Comment on any
Physics Today article.

The article does not have any references.

By the act of hitting a ball with a bat, one calculates the force energy to deliver the ball to its new location, but one must also take into account that the ball extended its energy to the entire team. Therefore the parameters of the damage extend into the future when the received energy to that pushed upon, later becomes released in a new event. Perhaps calculations of one added that in while another's calculations did not. E.M.C.
Written by Edgar McCarroll, 14 July 2012 19:59

Measured energy in Japan
David von Seggern
(vonseg@seismo.unr.edu) University of Nevada
July 2012, page 10
DIGITAL OBJECT IDENTIFIER
<http://dx.doi.org/10.1063/PT.3.1619>

The article by Thorne Lay and Hiroo Kanamori is an excellent review of the relationship between seismic moment and energy release. However, if the authors were consistent, they would find that the relationship between seismic moment and energy release is not linear. A 100-megaton nuclear explosion releases five times as much energy as a 20-megaton explosion, while that of a 300-megaton nuclear explosion releases approximately five times as much energy as a 60-megaton atmospheric explosion. The 1964 Chilean earthquake had still more energy by a factor of about 3, or 15 times that of a 100-megaton nuclear device. I believe the authors used the relation for seismic energy release rather than total strain energy release. Accounting for total strain energy release would increase the earthquake energy number by orders of magnitude. Despite the catastrophic damage potential of nuclear bombs, the forces of nature occasionally unleash much larger energy releases. Although the nuclear bombs are under our control, earthquakes, volcanic eruptions, and extreme weather events are not. However, by judicious preparation and avoidance measures, humans can significantly diminish the damage of natural events.

Molecular dynamics simulation of radiation damage in CaCd_6 quasicrystal cubic approximant up to 10 keV

P. H. Chen,^{1,3,a)} K. Avchachov,¹ K. Nordlund,¹ and K. Pussi²

¹Accelerator Laboratory, University of Helsinki, P.O. Box 43, 00014 Helsinki, Finland

²Department of Mathematics and Physics, Lappeenranta University of Technology, P.O. Box 20, FIN-53851 Lappeenranta, Finland

³Science and Technology on Surface Physics and Chemistry Laboratory, P.O. Box 718-35, 621907 Mianyang, China

(Received 16 April 2013; accepted 31 May 2013; published online 21 June 2013)

Due to the peculiar nature of the atomic order in quasicrystals, examining phase transitions in this class of materials is of particular interest. Energetic particle irradiation can provide a way to modify the structure locally in a quasicrystal. To examine irradiation-induced phase transitions in quasicrystals on the atomic scale, we have carried out molecular dynamics simulations of collision cascades in CaCd_6 quasicrystal cubic approximant with energies up to 10 keV at 0 and 300 K. The results show that the threshold energies depend surprisingly strongly on the local coordination environments. The energy dependence of stable defect formation exhibits a power-law dependence on cascade energy, and surviving defects are dominated by Cd interstitials and vacancies. Only a modest effect of temperature is observed on defect survival, while irradiation temperature increases lead to a slight increase in the average size of both vacancy clusters and interstitial clusters. © 2013 AIP Publishing LLC. [<http://dx.doi.org/10.1063/1.4811183>]

I. INTRODUCTION

The crystal structure has a strong influence on damage production in materials. Irradiated materials with different symmetries usually have different radiation tolerances.^{1,2} For example, aluminum and silicon have nearly the same mass, and differ by only 20% in atomic density, but their damage production appears quite different due to the different crystal structures in the following aspects:^{1,3} subcascade formation threshold energy, defect clusters structures, and regeneration rate of damage. In diamond structure silicon, amorphous clusters are usually produced in the cascade core, whereas in face-centered-cubic (fcc) aluminum, most of the crystal regenerates quickly and leaves only small vacancy-rich clusters. Besides, the size distribution of defect clusters also strongly depends on the crystal structure due to the different mobility of defects. For example, the size of defect clusters produced in fcc copper⁴ is much larger than that in body-centered-cubic (bcc) iron⁵ even with the same primary knock-on atom (PKA) energy. These differences may arise from the large number of close-packed directions in the fcc structures, i.e., the interstitial atoms and vacancies can migrate easily along these directions during and immediately after the thermal spike. Moreover, the form of the defect clusters also strongly depends on the crystal structure. In hexagonal closed-packed (hcp) zirconium and titanium, for instance, small defect clusters can be formed as a triangular arrangement of closely packed atoms within one basal plane occupying a smaller number of lattice position.^{6,7} In bcc iron, small clusters usually have a more open, three-dimensional structure.⁸

The concept of quasicrystals was first introduced in 1984.⁹ A quasicrystal has perfect long-range order, but no three-dimensional translational periodicity. As noted above, the damage production in a quasicrystal may differ a lot from that in a regular crystal due to the lack of translational symmetry. Additionally, the results of irradiation experiments using electrons and ion beams on quasicrystals have demonstrated that there is an irradiation-induced crystalline-quasicrystalline-amorphous phase transformation.¹⁰⁻¹³ However, it is nearly impossible to experimentally study this irradiation process on the atomic scale as it usually happens over several ns. Besides, most of the experimental works on irradiation effects in quasicrystals were performed at higher energies (from several hundreds of keV to GeV). It is difficult to experimentally study the irradiation effects at several keV due to the extremely short penetration distance (usually less than several nm). The PKA energies used in this work are lower than those used in experiments, but this allows the simulation of a collision from a secondary recoiled atom and also gives insight into how the PKA energy influences the damage. Computer simulations by molecular dynamics (MD) have been employed to understand the nature of the damage produced by fast atomic particles in materials ranging from metals^{1,14,15} to ceramics¹⁶⁻¹⁸ in the last two decades, and have clarified many important details of the evolution of collision cascades. Such knowledge is crucial for accessing the lifetime of materials in irradiation environment. To authors' knowledge, little work has been done on cascade simulation in quasicrystals due to their complex structures. As a first step, radiation damage in CaCd_6 binary quasicrystal is studied in the present paper.

The rest of this paper is organized as follows. In Sec. II, we present the structures and the interatomic potentials used.

^{a)}Electronic mail: chenph@live.cn

In Sec. III, we present the calculated results of the displacement threshold energy (E_d) and the evolution of defects during cascade simulations. Section IV concludes the present work.

II. COMPUTATIONAL MODELS

A. The structure of CaCd_6 quasicrystal approximants

The thermodynamically stable binary quasicrystals in the Ca-Cd systems, as well as many of their periodic approximants, can be described as packings of essentially identical clusters plus some extra glue atoms in between.¹⁹ The classic approximant to the $\text{CaCd}_{5.7}$ quasicrystals is the long known CaCd_6 phase, which is a more closely related approximant to the $\text{CaCd}_{5.7}$ quasicrystals than any other so far known.²⁰ In this work, the cubic 1/1-approximant CaCd_6 was used in the MD simulations. The primitive cell of CaCd_6 quasicrystal approximant is presented in Fig. 1. Each cell contains a total of 168 atoms. In the cubic CaCd_6 , the clusters are arranged on a bcc lattice. The structures of the quasicrystal approximants play a key role in understanding quasicrystals, since they are expected to display the same local arrangements as the true quasicrystal.²⁰

B. Potentials

The empirical embedded atom method (EAM) potentials developed by Brommer²¹ for CaCd_6 quasicrystal approximant, which was derived using a forcing-match method and shows comparable results with the experiments, were used. For use in collision cascades simulation, the EAM potentials were at small distances joined to the Ziegler-Biersack-Littmark (ZBL) pair potential to model the highly repulsive nuclei-nuclei interaction using the Fermi function

$$V_{tot}(r) = V_{ZBL}(r)(1 - F(r)) + V_{Eq}(r)F(r),$$

where V_{tot} , V_{ZBL} , V_{Eq} , and r are the total potential energy, universal ZBL repulsive potential, original pair part of EAM potential, and distance between atoms, respectively. The Fermi function is defined as

$$F(r) = 1/(1 + e^{-b_f(r-r_f)}),$$

where b_f and r_f are adjustable parameters. The values of b_f and r_f are chosen such that the potential is essentially unmodified at the equilibrium and longer bonding distances, and are chosen to be 10, 2.6 Å for Ca and 10, 2.25 Å for Cd, respectively. The electronic density function is truncated for smaller distances. At distances shorter than r_f , the electronic density is constant.

Moreover, the melting temperature is especially important to cascade simulations with energies above 1 keV, where local atoms will have strongly disordered configurations, which would have some similarity to structures at high temperatures. With the present potential, the melting point was evaluated to be 880 K by calculation of the T-t (Temperature-time) curve for a crystal while it is heated from solid to liquid, as described by Osetsky and Serra.²² The behaviour of this potential somewhat overestimates the melting point when comparing with experiment, where a value of 838 K is given.²³

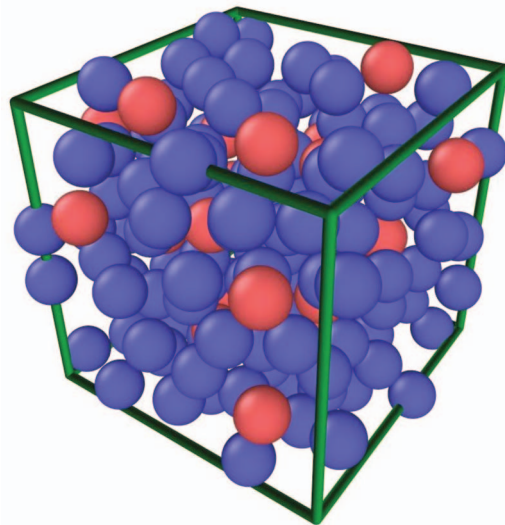


FIG. 1. The primitive cell of CaCd_6 quasicrystal approximant. The structure was taken from the alloy database at <http://alloy.phys.cmu.edu>.

The direct heating method, however, is known to overestimate the melting point, as without a seed for melting it leads to superheating.^{24,25} In normal metals with close-packed structures, this superheating is typically about 15%. However, in the current case with weakly ordered quasicrystals, it is likely less. In any case we can conclude that the simulated melting point of the interatomic potential is within $\sim 10\%$ of the experimental value.

C. Damage analysis methods

In simple crystals there are many well-established ways for analysing damage, such as using Wigner-Seitz cells, spheres centered on lattice atoms, potential energy,¹ short-range order parameters,²⁶ and angular structure factors.²⁷ Analysing for damage in a quasicrystal is somewhat challenging, as the atoms have many different bonding environments, and hence some of the conventional methods may not work. For instance, as atoms have a different number of neighbours, a short-range order approach would not be straightforward to use. Similarly, we found that the number of different angles between bonds is too large for angular damage analysis to be practical.

For the current work, we found that two approaches were practically useful for damage analysis. The methods chosen were potential energy and Voronoi cell analysis.¹ In the potential energy method, those atoms with a potential energy higher than the equilibrium value were labelled as defects. This is a convenient way to identify the damage zones, but it does not give detailed information on the defect structures on an atomic level. The Voronoi cell method²⁸ was used to recognize interstitials and vacancies by analysing the atom positions with respect to the lattice defined by the original undisturbed simulation cell. A lattice site with an empty Voronoi cell was labelled a vacancy and a cell with multiple atoms an interstitial. Since irradiation damage in quasicrystals has not been analysed earlier, we report results for both methods to allow comparison.

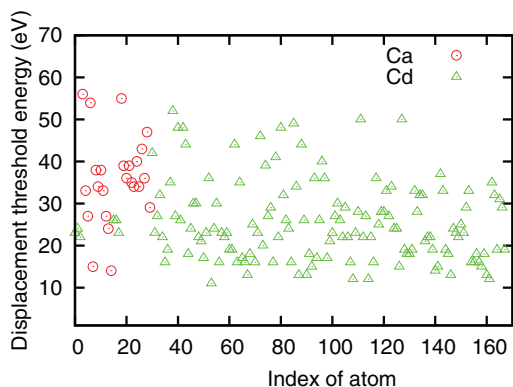


FIG. 2. Displacement threshold energies of atoms along the [1 0 0] direction.

III. RESULTS AND DISCUSSION

A. Displacement threshold energies

The displacement threshold energies' calculation is based on the method presented by Nordlund²⁹ with a search increment step of 1 eV. The Voronoi method was used to identify the defects. First, a fixed PKA direction is used, namely [1 0 0], at 0 K for all the 168 atoms in the primary cell. Second, the displacement threshold energy surface for all lattice directions of one atom was calculated. All the calculations were carried out using the LAMMPS code³⁰ with the initial temperature of 0 K under the constant number, volume, and energy (NVE, microcanonical) ensemble and periodic boundary conditions. A $6 \times 6 \times 6$ supercell (36 288 atoms) was used for all the calculations. A variable time step, which is dependent on the maximum velocity and interaction force in the system, was applied.

The evaluated E_d is shown in Fig. 2. The threshold displacement energy varied considerably depending on the local bonding structures. No significant dependency of the displacement threshold energy on the atom types was found.

Fig. 3 shows the three-dimensional threshold displacement energy surface $E_d(\theta, \phi)$ of one Ca atom in the CaCd₆ quasicrystal approximants. The average threshold displacement energy is 29 eV. There seem to be strong anisotropies. In some high- E_d cases, creation of several defects immediately

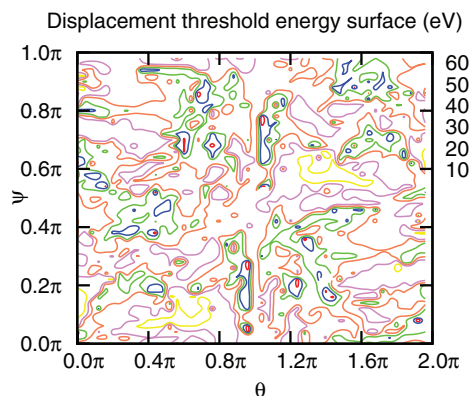


FIG. 3. Contour plots of the three-dimensional threshold displacement energy surface of one atom.

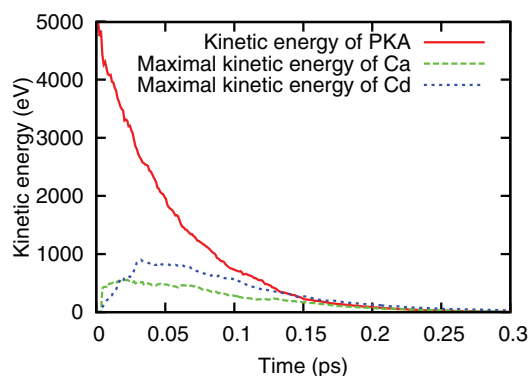


FIG. 4. Time dependence of the energy of PKA and the maximum energy of Ca and Cd recoils.

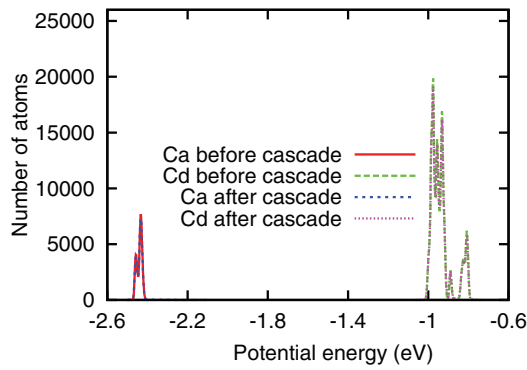
above the threshold was observed. The behaviour of other atoms is very similar.

B. Displacement cascade simulation

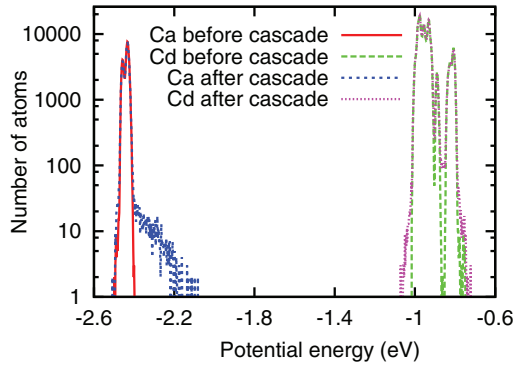
Displacement cascades were triggered by introducing an excess energy to an atom at 0 K and 300 K and for a PKA energy of 1–10 keV. The atoms in the outermost three layers are coupled to a heat bath to maintain a constant temperature. The initial velocity direction of the recoil atom was chosen randomly. In each case, at least 5 simulations were performed in order to obtain representative statistics. Additional cascades were differentiated by changing the location of the PKA atom or by using a different equilibrated atom block.

Fig. 4 shows the time dependence of the energy of PKA and the maximum energy of Ca and Cd among all the atoms included in the simulation box with an energy of 5 keV. In this case, 100 simulations with different initial velocity directions are performed and averaged. The PKA lost more than 90% of the initial energy within 0.2 ps, and the maximum energy of Ca is lower than that of Cd. The lower concentration of Ca in CaCd₆ may account for the lower energy transfer. Another possible reason is that the mass of Ca is smaller than that of Cd, and then a Ca can get away from the PKA before collision.

The potential energy distributions before and after a cascade with an energy of 10 keV at 0 K are presented in Fig. 5. Fig. 6 shows the time dependence of the number of defects defined by these two damage analysis methods in displacement cascade with energies of 1, 2, 5, and 10 keV at 0 K. In each case, 5 simulations with different initial velocity directions are performed and averaged. For any given event, the amount of damage at the end of the cascade obtained according to potential energy is roughly 1.6 times that by the Voronoi method. In all four figures, cascades have similar behaviour with an increase in the number of defects during the ballistic phase, followed by a rapid decrease during the cooling stage and stabilisation in a further relaxation stage. The rapid decrease corresponds to recombination of an interstitial atom with the vacancy to which the interstitial initially belonged. Collision cascades at an energy of 10 keV have been shown to be broken up into spatially separated subcascades. When the zones cool down, they form amorphouslike



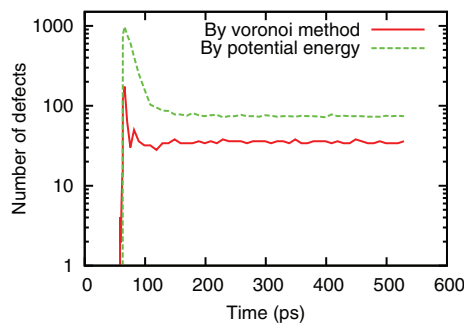
(a)



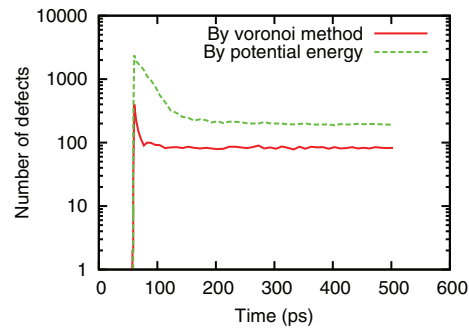
(b)

FIG. 5. Potential energy distributions before and after cascade with an energy of 10 keV at 0 K: (a) in the linear scale and (b) in the log scale.

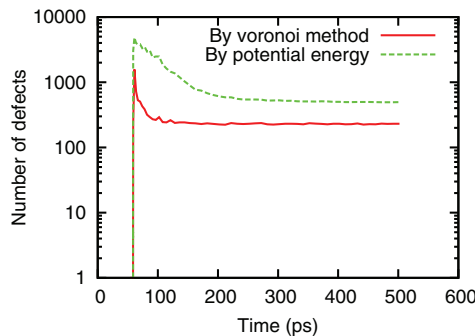
damage pockets. Animations of 8 and 9 keV cascades showed that the former were not broken down into subcascades, while the latter were, indicating that the threshold for subcascade formation in CaCd₆ quasicrystal is about 8 keV at 0 K.



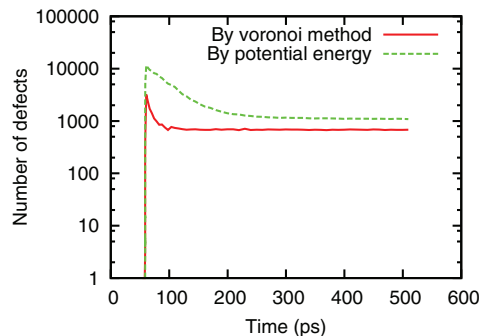
(a)



(b)



(c)



(d)

FIG. 6. Time dependence of the number of defects defined by both potential energy and the Voronoi method: (a) 1 keV; (b) 2 keV; (c) 5 keV; and (d) 10 keV.

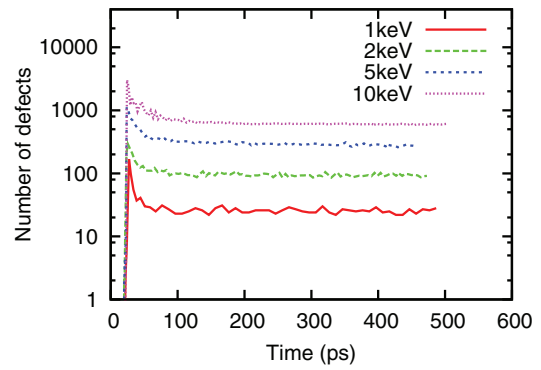


FIG. 7. Time dependence of the number of defects at 300 K.

Fig. 7 shows the evolution of the number of defects in displacement cascade with energies of 1, 2, 5, and 10 keV at 300 K defined by the Voronoi cell method. Table I gives results for the number of interstitial and replacement atoms survived at the end of cascade simulations with energies from 1 to 10 keV at 0 and 300 K. Increasing temperature leads to a slight increase in the number of defects. The effect of lattice temperature on the number of defects is rather weak below 2 keV. Since one cascade produces fewer defects on average than two separate cascades of the total energy, the difference at an energy of 10 keV becomes small when subcascade formations occur at 0 K, but is not observed at 300 K. The number of Ca atoms remaining as interstitials at the end of cascade is about one tenth of the number of Cd atoms. The possible reason attributed to this is the lower concentration and the lighter mass of Ca atoms.

The number of stable defects (N_D) remaining at the end of cascade simulations with energy from 1 keV to 10 keV at 0 K by the Voronoi method are presented in Fig. 8. It

TABLE I. Number of interstitial and replacement atoms survival at the end of cascade simulations with energies from 1 to 10 keV at 0 and 300 K. I_{Ca} is the number of Ca interstitials, I_{Cd} is the number of Cd interstitials, R_{Ca} is the number of Ca atoms in Cd site, and R_{Cd} is the number of Cd atoms in Ca site.

Energy (keV)	0 K				300 K			
	I_{Ca}	I_{Cd}	R_{Ca}	R_{Cd}	I_{Ca}	I_{Cd}	R_{Ca}	R_{Cd}
1	2	31	26	25	2	26	41	39
2	4	71	93	101	9	82	102	93
5	17	210	261	254	18	252	329	312
10	60	523	690	638	59	554	663	632

exhibits a power-law dependence on cascade energy and can be expressed as

$$N_D = (35.95 \pm 1.25) \times E_{MD}^{1.171 \pm 0.024},$$

where the cascade energy, E_{MD} , is given in keV. At each energy, the data point is an average of 5 cascades. As a result of subcascades, N_D begins to deviate from this energy dependence above 9 keV when subcascade formation occurs. Subcascade formation would lead to an increase in the gradient of the plot in Fig. 8 due to the formation of slightly disordered atom regions between subcascades. These relatively low defect density zones which connect the dense subcascades could present higher defect survival efficiencies and then raise the number of surviving defects. For higher PKA energies (several hundreds of keV) where subcascade formation becomes prominent, it is expected that the defect number should then simply be the sum of N_D for lower energy events. The exponent m in the power-law relationship is about 1.17, which is larger than that for most crystalline materials where it is ≤ 1.0 .²

C. Final state of damage

The final damage produced by cascades was also analysed. All defects (Voronoi) which were neighbours of each other in Voronoi analysis were interpreted to be adjacent. All

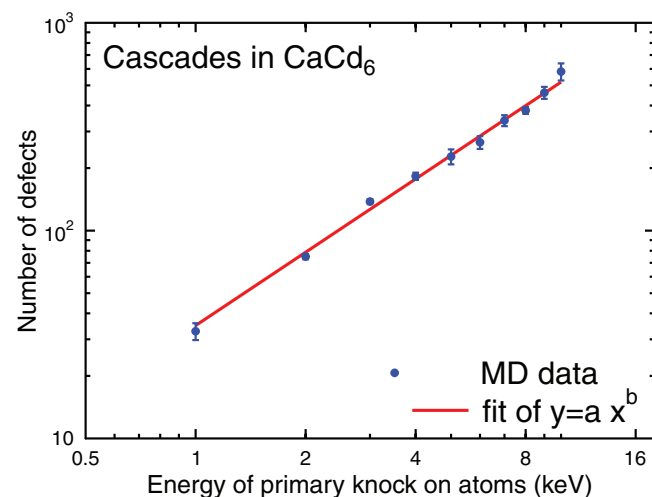


FIG. 8. Log-log plots of the number of defects as a function of the energy of primary knock on atoms at 0 K.

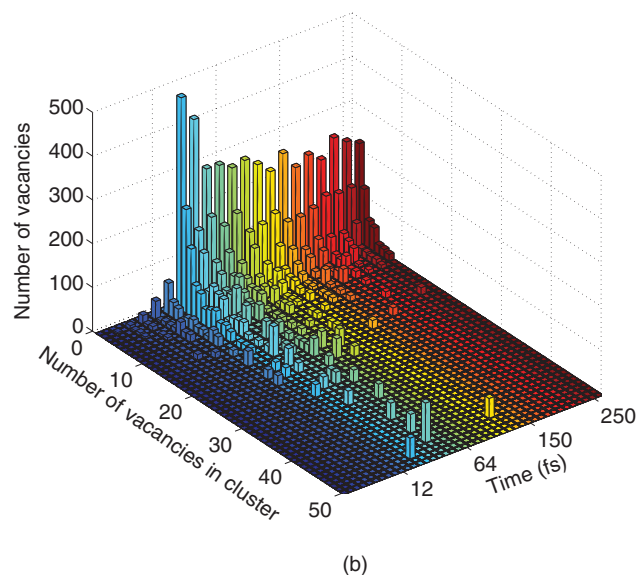
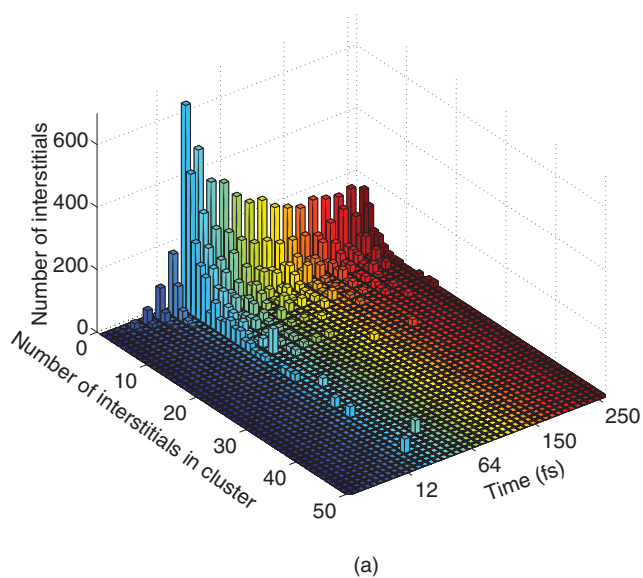


FIG. 9. Distribution of Voronoi defects as a function of cluster size for 10 keV recoil at 0 K. (a) Interstitials. (b) Vacancies.

defects within the same network of adjacent defects were interpreted to form one cluster. Fig. 9 shows the size distributions of vacancies and interstitial clusters as a function of time with an energy of 10 keV at 0 K. The vacancy cluster distribution reaches a stable value in about 50 fs, while the interstitial clusters continue to change for a few hundreds of fs after the initiation of the cascade due to the low migration energy of interstitials.

Fig. 10 shows the size distributions of vacancies and interstitial clusters of the final damage as a function of energy at 0 K. Both the interstitial and vacancy cluster size distributions shift to larger sizes with the cascade energy. There is a systematic change in the cluster size distribution, with higher energy cascades producing larger clusters.

Fig. 11 shows the size distributions of vacancy and interstitial clusters of the final damage at 0 and 300 K with a PKA energy of 10 keV. At elevated temperature, the vacancies and interstitials both tend to produce larger clusters. An

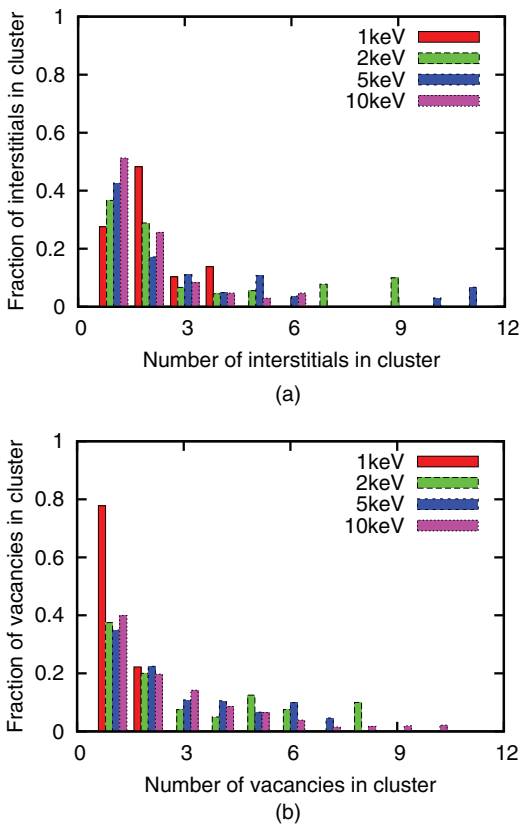


FIG. 10. Distribution of Voronoi defects as a function of cluster size with different energies at 0 K. (a) Interstitials. (b) Vacancies.

increase in the clustering fraction at the higher temperatures is most clearly seen as a decrease in the number of mono-interstitials. A comparison of Figs. 11(a) and 11(b) indicates that the average size of vacancy clusters is larger than that of interstitials. The atoms that are unable to regain lattice sites during this final stage become self-interstitial atoms at the periphery of the core, whereas vacancies are dragged into the center of the liquid when it contracts.³¹ Isolated point defects are predominantly interstitials far from the cascade core, and the damage in the cores is vacancy rich. Individual replacement collision sequences (RCSs; Fig. 12) can be ejected early on during the ballistic phase, but self-interstitial atoms created by these events represent only a minor part of the total population of Frenkel pairs produced by cascades at lattice temperatures where focused chains are difficult to establish.

Replacement collision sequences, which can produce interstitial atoms outside the liquid core of the cascade, were also observed in CaCd_6 quasicrystal at 300 K as seen in Fig. 12. The image shows a 25 nm thick cross section of the simulation cell at 500 ps after the initiation of the cascade. The replacement collision sequences are visible as straight rows of displaced atoms around the heat spike core. The replacement collision sequences typically have lengths of 6 lattice constants, and some interstitials appear to be produced without any visible RCSs. One of the most striking results of this work is the fact that few isolated Frenkel pairs are produced directly by the displacement cascades, while the RCSs have extremely long atomic replacements. The largest defect clusters are clearly disordered (amorphous) atom zones (see

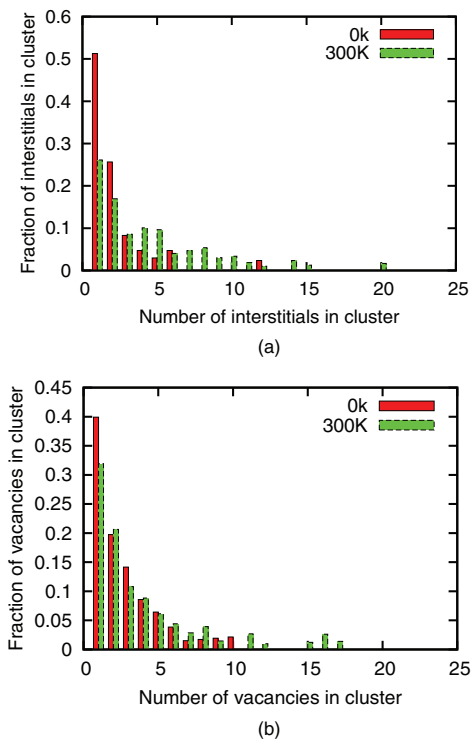


FIG. 11. Distribution of Voronoi defects as a function of cluster size at 0 and 300 K with a PKA energy of 10 keV. (a) Interstitials. (b) Vacancies.

Fig. 12), similar to the amorphous defect zones often observed in semiconductors after irradiation.^{32,33} Hence the current results indicate that ion irradiation can be used to introduce localized amorphous regions in quasicrystals. Their stability on macroscopic time scales cannot be determined from the current work due to the limited time scale of MD simulations, but considering that many metal alloys can form macroscopic stable amorphous metals, it is reasonable to assume that at least in some quasicrystals the amorphous pockets may be stable.

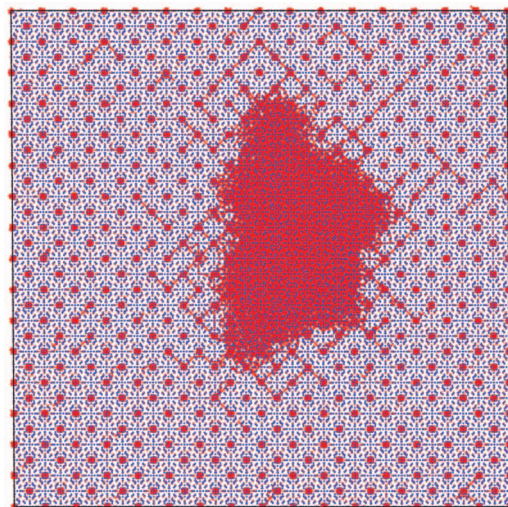


FIG. 12. Defects produced by replacement collision sequences with a PKA energy of 10 keV at 300 K; red lines represent the displacement of atoms.

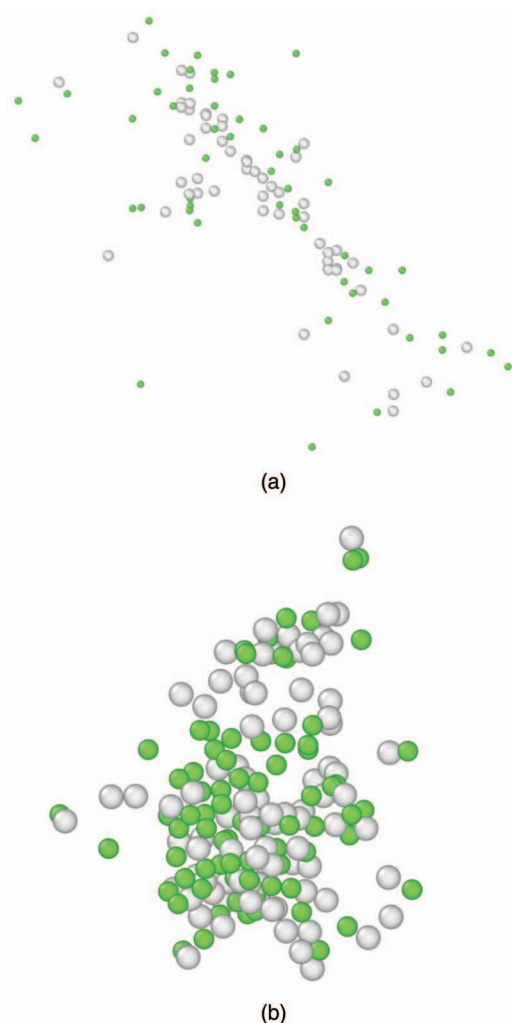


FIG. 13. Final damage state with a PKA energy of 2 keV at 0 K: (a) fcc Ca and (b) CaCd₆. White (larger) spheres represent vacancy and green (smaller) spheres represent interstitial.

D. Comparison with fcc Ca

The final damage states of a typical 2 keV cascade in fcc Ca and CaCd₆ quasicrystal at 0 K are shown in Figs. 13(a) and 13(b), respectively, where only defects are presented. The vacancies are represented by large spheres and the interstitials are represented by small ones, as indicated in the legend. Analysis of the defect clusters in fcc Ca using the same way as the analysis of CaCd₆ showed that they were in all cases either pure vacancy or pure interstitial clusters. The small size and simple nature of the clusters in fcc Ca compared to CaCd₆ reflect the importance of the crystal regeneration effect in fcc metals. In CaCd₆ quasicrystal, amorphous clusters are produced in the cascade cores, whereas in fcc Ca, most of the crystal regenerates, leaving only small defect clusters in the final damage state. The size of defect clusters is clearly larger in CaCd₆ quasicrystal than in fcc Ca due to the difference in structures. There are two possible mechanisms that account for the formation of interstitial clusters. First, clusters can form quite early in the cascade process during the transition from the ballistic collision phase to the thermal spike phase. Second, they can also be generated due to the migration of

atoms in the vicinity of the heat spike after the collision stage. The damage structure of 5 keV cascades in CaCd₆ quasicrystal was studied and found that annealing a cascade at 700 K for 200 ps only leads to very slight changes in defect size and cascade morphology, so it is concluded that most of the interstitial clusters are created during the cooling stage. Meanwhile, most of the isolated interstitial clusters in fcc Ca can be removed by annealing at 700 K for 200 ps, indicating that interstitial clusters in fcc Ca are mainly generated due to defect diffusion during the thermal spike. The behaviour of fcc Ca is similar to other elemental metals, in which the translational symmetry and close-packed structure make for efficient damage recombination¹ and enables easy long-range defect migration that enhances the damage recombination. As the quasicrystal structures do not have translational symmetry and are not close-packed, the damage does not have the same ability to regenerate, leading to the formation of large amorphous regions.

IV. CONCLUSIONS

A molecular dynamics method has been used to study the defect production in CaCd₆ quasicrystal. The displacement threshold energies depend surprisingly strongly on the local coordination environments. No significant dependency of displacement threshold energy on the atom types was found. The number of stable defects remaining at the final stage with energy from 1 keV to 10 keV at 0 K shows a power-law dependence on cascade energy. The exponent m in the power-law relationship is larger than that for most crystalline materials. The results on final damage produced by cascades with different PKA energies at different temperatures show that both the interstitial and vacancy cluster sizes' distribution shifts to larger sizes with an increasing of PKA energy and temperature. Most of the interstitial clusters are created during the transition from the ballistic collision phase to the thermal spike phase, while most of the isolated interstitial clusters in fcc Ca are mainly formed by defect diffusion during the thermal spike.

ACKNOWLEDGMENTS

This work was partially financially supported by the Science and Technology Foundation of China Academy of Engineering Physics and the National Natural Science Foundation of China.

¹K. Nordlund, M. Ghaly, R. S. Averback, M. Caturla, T. Diaz de la Rubia, and J. Tarus, *Phys. Rev. B* **57**, 7556 (1998).

²D. J. Bacon, F. Gao, and Y. N. Osetsky, *J. Nucl. Mater.* **276**, 1 (2000).

³L. Pelaz, L. A. Marqués, M. Aboy, P. López, and I. Santos, *Eur. Phys. J. B* **72**, 323 (2009).

⁴R. E. Voskoboynikov, Y. N. Osetsky, and D. J. Bacon, *J. Nucl. Mater.* **377**, 385 (2008).

⁵J. W. Wang, X. C. Shang, and G. C. Lv, *Adv. Mater. Res.* **179**, 513 (2011).

⁶S. J. Wooding, L. M. Howe, F. Gao, A. F. Calder, and D. J. Bacon, *J. Nucl. Mater.* **254**, 191 (1998).

⁷S. J. Wooding, D. J. Bacon, and W. J. Phythian, *Philos. Mag. A* **72**, 1261 (1995).

⁸L. Malerba, *J. Nucl. Mater.* **351**, 28 (2006).

⁹D. Shechtman, I. Blech, D. Gratias, and J. W. Cahn, *Phys. Rev. Lett.* **53**, 1951 (1984).

- ¹⁰K. Urban, N. Moser, and H. Kronmüller, *Phys. Status Solidi A* **91**, 411 (1985).
- ¹¹G. W. Yang, W. S. Lai, C. Lin, and B. X. Liu, *Appl. Phys. Lett.* **74**, 3305 (1999).
- ¹²P. M. Ossi, *Radiation Effects in Solids* (Springer, 2007), p. 259.
- ¹³S. Mechler, C. Abromeit, N. Wanderka, M.-P. Macht, T. Zunkley, G. Schumacher, and S. Klaumzner, *Nucl. Instrum. Methods Phys. Res. B* **245**, 133 (2006).
- ¹⁴G. Ackland, D. Bacon, A. Calder, and T. Harry, *Philos. Mag. A* **75**, 713 (1997).
- ¹⁵L. A. Zepeda-Ruiz, S. Han, D. J. Srolovitz, R. Car, and B. D. Wirth, *Phys. Rev. B* **67**, 134114 (2003).
- ¹⁶L. Van Brutzel, J. M. Delaye, D. Ghaleb, and M. Rarivomanantsoa, *Philos. Mag.* **83**, 4083 (2003).
- ¹⁷B. P. Uberuaga, R. Smith, A. R. Cleave, G. Henkelman, R. W. Grimes, A. F. Voter, and K. E. Sickafus, *Phys. Rev. B* **71**, 104102 (2005).
- ¹⁸H. Tsuchihira, T. Oda, and S. Tanaka, *Nucl. Instrum. Methods Phys. Res. B* **269**, 1707 (2011).
- ¹⁹C. P. Gómez and S. Lidin, *Angew. Chem., Int. Ed.* **40**, 4037 (2001).
- ²⁰C. P. Gómez and S. Lidin, *Phys. Rev. B* **68**, 024203 (2003).
- ²¹P. Brommer, F. Gähler, and M. Mihalkovi, *Philos. Mag.* **87**, 2671 (2007).
- ²²Y. N. Osetsky and A. Serra, *Phys. Rev. B* **57**, 755 (1998).
- ²³J. Jiang, C. Jensen, A. Rasmussen, and L. Gerward, *Appl. Phys. Lett.* **78**, 1856 (2001).
- ²⁴J. R. Morris, C. Z. Wang, K. M. Ho, and C. T. Chan, *Phys. Rev. B* **49**, 3109 (1994).
- ²⁵K. Nordlund and R. S. Averback, *Phys. Rev. Lett.* **80**, 4201 (1998).
- ²⁶P. Erhart, A. Caro, M. Caro, and B. Sadigh, *Phys. Rev. B* **77**, 134206 (2008).
- ²⁷H. Zhu, R. S. Averback, and M. Nastasi, *Philos. Mag. A* **71**, 735 (1995).
- ²⁸Z. Masáková, J. Patera, and J. Zich, *J. Phys. A* **36**, 1869 (2003).
- ²⁹K. Nordlund, J. Wallenius, and L. Malerba, *Nucl. Instrum. Methods Phys. Res. B* **246**, 322 (2006).
- ³⁰S. Plimpton, *J. Comput. Phys.* **117**, 1 (1995).
- ³¹K. Nordlund and R. S. Averback, *Phys. Rev. B* **59**, 20 (1999).
- ³²M. O. Ruault, J. Chaumont, J. M. Penisson, and A. Bourret, *Philos. Mag. A* **50**, 667 (1984).
- ³³M. W. Bench, I. M. Robertson, M. A. Kirk, and I. Jenčič, *J. Appl. Phys.* **87**, 49 (2000).